Journal of Hydrology 620 (2023) 129527

Contents lists available at ScienceDirect

Journal of Hydrology

journal homepage: www.elsevier.com/locate/jhydrol

Research papers

Evaluating subsurface flow connectivity in a pine-covered hillslope with stemflow infiltration and ground-penetrating radar surveys

Simone Di Prima [a,*], Gersende Fernandes [b], Elisa Marras [c], Filippo Giadrossich [c], Ryan D. Stewart [d], Majdi R. Abou Najm [e], Thierry Winiarski [b], Brice Mourier [b], Rafael Angulo-Jaramillo [b], Alessandro Comegna [a], Antonio del Campo [f], Laurent Lassabatere [b]

[a] School of Agricultural, Forestry, Food and Environmental Sciences (SAFE), University of Basilicata, 85100 Potenza, Italy
[b] Univ Lyon, Université Claude Bernard Lyon 1, CNRS, ENTPE, UMR5023 LEHNA, F-69518, Vaulx-en-Velin, France
[c] Nuoro Forestry School, Department of Agricultural Sciences, University of Sassari, Viale Italia, 39A, 07100 Sassari, Italy
[d] School of Plant and Environmental Sciences, Virginia Polytechnic Institute and State University, Blacksburg, VA, United States
[e] Department of Land, Air and Water Resources, University of California, Davis, CA 95616, United States
[f] Research Group in Forest Science and Technology (Re-ForeST), Universitat Politècnica de València, Camí de Vera, E-46022 València, Spain

ARTICLE INFO

This manuscript was handled by Corrado Corradini, Editor-in-Chief, with the assistance of Wei Hu, Associate Editor

Keywords:
GPR
Connectivity
Water infiltration
Stemflow
Preferential flow

ABSTRACT

The hydrological response of sloping catchments is strongly conditioned by the connectivity of subsurface preferential flows. The objective of this paper is to investigate the role played by stemflow infiltration in subsurface water flow dynamics, focusing on a forested hillslope located in an Aleppo pine Mediterranean forest (*Pinus halepensis*, Mill.) located at Sierra Calderona, Valencia province, Spain. We combined stemflow artificial experiments with the ground-penetrating radar (GPR) as a non-invasive technique to investigate stemflow-induced preferential flow paths activated by different trees and the related hydrological connectivity at the hillslope scale. Our observations allowed us to identify different dynamics associated with the initiation of stemflow and then lateral preferential flow, including the activation of connected preferential flow paths that received stemflow water from different trees. These observations provided empirical evidence of the role of stemflow in the formation of lateral preferential flow networks. Our measurements also provided estimations for flow velocities, which provided new insight on the magnitude of stem-induced lateral preferential flow paths. The applied protocol offers a simple, repeatable and non-invasive way to conceptualize hillslope responses to rainstorms.

1. Introduction

Changing climatic conditions are threatening the health and longevity of many forests, while also affecting related hydrological and biogeochemical processes (Calheiros et al., 2021). Optimizing the remanence and longevity of forests is of prime ecological importance. In fact, forests play a crucial role in hydrological and biogeochemical processes. Forests regulate water access to the soil surface and infiltration into the soil profile. Tree canopies partition the incident gross precipitation into three components: i) the intercepted rainfall that is lost by evaporation directly from the canopies, ii) the throughfall that passes through the canopies and reaches the soil surface, and iii) the stemflow that is concentrated from the canopies to the stems (Llorens and Domingo, 2007).

Investigations from different environments and forest types reported that stemflow often preferentially infiltrates around the stem base and once belowground becomes funneled by tree roots (Levia and Frost, 2003). This two-stages water flow process, which starts with the formation of the stemflow aboveground and continues with the redistribution of the infiltrated water in the subsurface, is known as the "double-funneling" effect (Johnson and Lehmann, 2006). Following this concept, the trees may be regarded as hydrologically-active agents, with their tree roots constituting initiation points from which preferential flow paths can originate (Uchida et al., 2001).

During particularly intense rainstorms, as large volumes of stemflow are funneled by the roots these paths may connect together in a subsurface flow network that controls the hydrological response of the hillslope (Lehmann et al., 2007). This subsurface water dynamic agrees

* Corresponding author.
E-mail address: simone.diprima@unibas.it (S. Di Prima).

https://doi.org/10.1016/j.jhydrol.2023.129527
Received 6 January 2023; Received in revised form 11 April 2023; Accepted 12 April 2023
Available online 17 April 2023

with the connect-and-react mechanism proposed by Bachmair and Weiler (2011), and it is behind the flashy response observed in some steep forested hillslopes (e.g., Schwärzel et al., 2012). Although previous work has highlighted the importance of this process and of the degree of connectivity in determining the hillslope's response to rainstorms, until now the formation of stemflow-induced preferential flow paths has mainly been investigated at the scale of the single tree (e.g., Guo et al., 2020).

In this work, we investigated this process at the hillslope scale by performing an artificial stemflow experiment on a steep, forested hillslope located in the Valencia province (Spain), in the Sierra Calderona Natural Park. The site was chosen because previous studies provided evidence of later subsurface flow occurrence and hypothesized the presence of preferential flow networks determining the rapid response of the hillslope (del Campo et al., 2019). However, the factors involved in the initiation of the process remain poorly investigated. The aim of our study was to bridge this gap focusing on stemflow infiltration as a main factor of preferential flow initiation. To gain insight on subsurface water dynamics we combined time-lapse ground penetrating radar (GPR) surveys with stemflow simulations involving three rows of trees separated by a few meters. To interpret the results we designed a protocol to detect stemflow-induced preferential flow paths activated by the trees. We then generalized our results to better understand hydrological connectivity at the hillslope scale.

2. Material and methods

2.1. Experimental site and artificial stemflow experiment

The Calderona site (39°42′29″N, 0°27′25″W) is an Aleppo pine (*Pinus halepensis* Mill.) semiarid forest located in the Valencia province (East Spain), in the Sierra Calderona Natural Park. This experimental site was previously the location of an assessment of ecohydrological effects of forest management (del Campo et al., 2018). Two plots of the forest underwent contrasting treatments after a wildfire occurred in 1992. The first was allowed to evolve naturally by ecological succession. The second was planted and tree density was controlled.

The climate is characterized by high temporal rainfall variability and intense droughts. The mean annual temperature is 14.0 °C, while the mean annual rainfall is 342 mm, with rainfall events scattered along the year and mainly associated to convective rainfall (del Campo et al., 2018). The soil is loamy textured and relatively shallow (10–40 cm), and has a basic pH and a high calcium carbonate content. The last forest management occurred between January and October 2012. The objective of the treatment was to achieve a homogeneous forest cover distribution by removing double-stemmed trees and the trees with smaller diameters. The tree density reduction was 94 %, with a total basal area removal of 74 %. More details about the forest stand can be found in del Campo et al. (2018).

The field experiment used simulated stemflow events to provide evidence of stemflow-induced preferential flow pathways and flow connectivity. The experiment was conducted in October 2021, which is a favorable period to high intensity rainfall (Camarasa-Belmonte and Soriano, 2014). The initial soil water content was determined to be 0.20 $cm^3\ cm^{-3}$ via the gravimetric method on undisturbed soil cores (~100 cm^3).

We firstly selected a 100 m^2 subplot area within the treated plot that included eight Aleppo pine trees. Two trees (named Trees 1 and 2) were located in the upper part of the subplot, three trees (Trees 3, 4 and 5) were located in the central part, and three trees (Trees 6, 7 and 8) were located in the lower part (Fig. 1). To setup the artificial stemflow experiment on each tree, we followed the procedure described in Guo et al. (2020) and Di Prima et al. (2022). The water application was carried out using a PVC pipe with a 1-mm-diameter hole every 50 mm (Fig. 2c). The pipe was connected to a plastic funnel and positioned around the tree trunk at 0.2 m from the soil surface (Fig. 2a).

Water application in the experiment consisted of two stages (Fig. 3). In the first stage, we applied 50 L of water to each trunk of Trees 1 and 2. During the second stage, the same amount of water was applied on the trunks of Trees 3, 4 and 5. This amount of water corresponded to the expected volume collected by a tree crown for a rainfall intensity of 40.4 mm h^{-1}, and represented a mean stemflow rate of 0.35 L mm^{-1} (stemflow volume drained per amount of precipitation) as estimated for the Calderona site by del Campo et al. (2018), and a duration of the simulated event of 3 h and 20 min. These features define a very strong rainfall event. However, the Mediterranean climate is known for its extreme rainfall events with common intensities over 100 mm h^{-1} at the storm peak (Camarasa-Belmonte and Soriano, 2014).

2.2. Time-lapse GPR surveys

Two cross-slope-oriented GPR survey lines were established in the subplot using measuring tapes (Fig. 2b), and following the sampling scheme reported in Fig. 1. The first survey line (SL1) had a length of 8.6 m and was placed on the downhill side of Trees 1–5 (Fig. 1), whereas the second survey line (SL2) had a length of 7.4 m and was placed on the

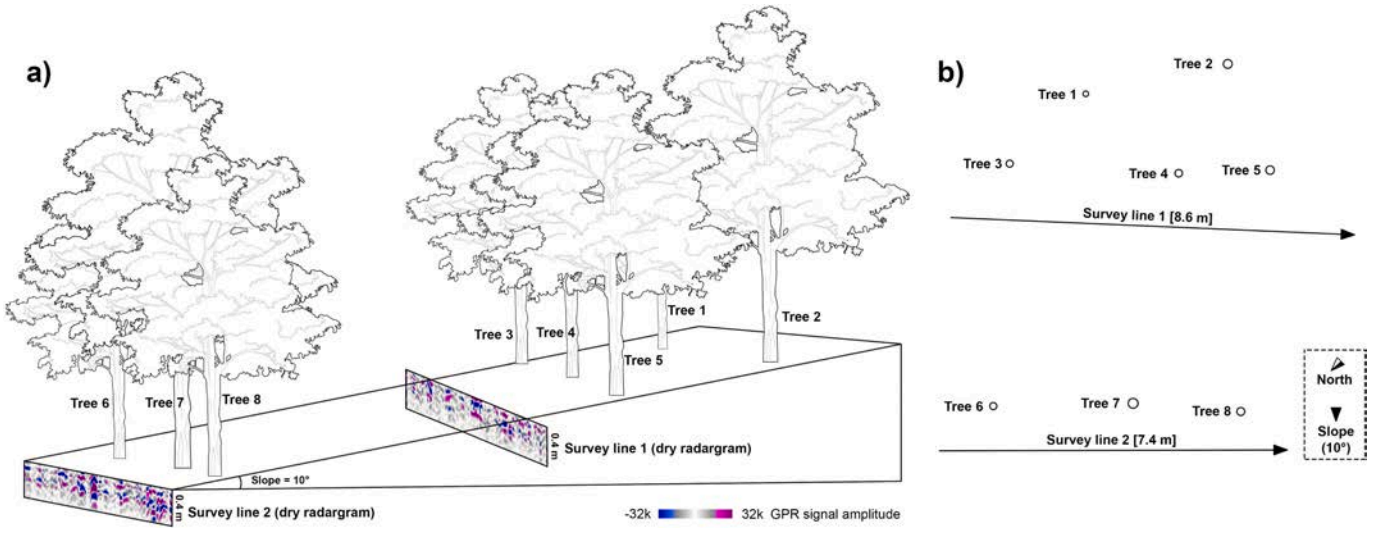

Fig. 1. Experimental setup at the Calderona site. (a): Position in the studied hillslope of the GPR survey lines along with the radargrams collected before the excution of the artificial steamflow experiment. (b): Scheme of the GPR survey.

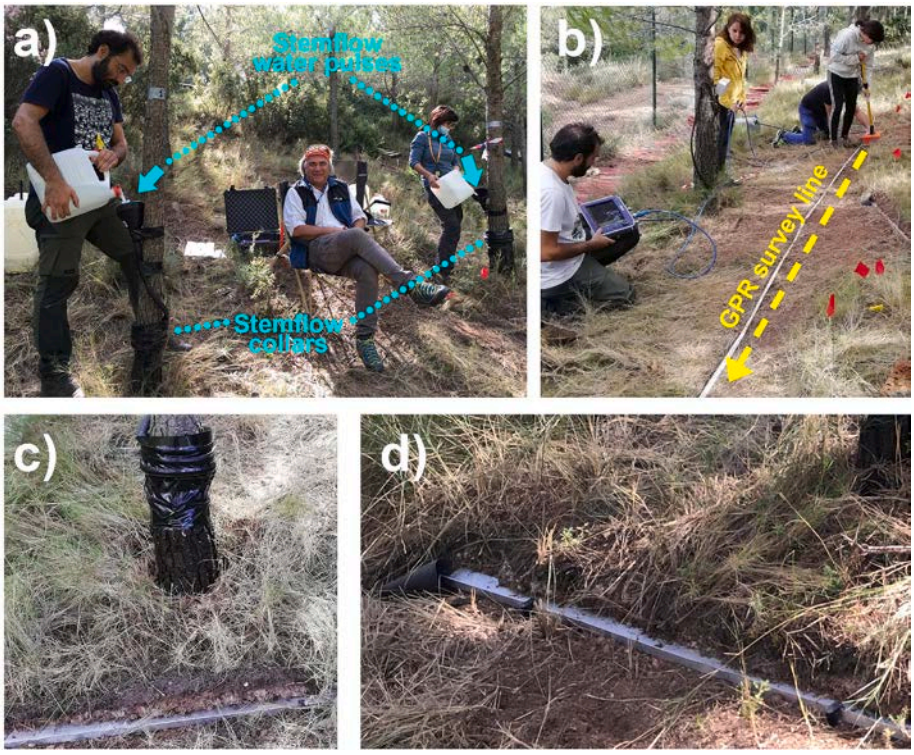

Fig. 2. (a): Stemflow water pulses poured on Trees 1 and 2. (b): GPR survey carried out on Survey line 2. (c): Stemflow collar. (d): Channel for collecting overland flow.

downhill side of Trees 6–8. The GPR surveys were carried out using a GSSI (Geophysical Survey System Inc., Salem, NH) SIR 4000 system with a 900-MHz antenna. A total of 22 radargrams (11 GPR surveys × 2 survey lines) were collected in time mode by moving the antenna along the survey lines and recording markers every 0.2 m of the measuring tapes (Fig. 2b). The first GPR survey was carried out just before the artificial stemflow events (radargrams in Fig. 1a), while the other 11 surveys were carried out during the experiment (Fig. 3a). This experimental design was aimed to detect stemflow-induced preferential flow paths activated by different trees and the related hydrological connectivity throughout the hillslope. Fig. 3a depicts the timeline of the artificial stemflow experiment with the stemflow volumes poured on the five selected trees through repeated pulses (blue lines). In the timeline are also visible the GPR surveys carried out on SL1 and SL2 (yellow lines).

The artificial stemflow experiment started after the first GPR survey, when the first water volumes were poured into the funnels (Fig. 2a). During this first stage, five stemflow pulses, each of 10 L, were poured into the funnels connected to Trees 1 and 2 at times of 0:00, 0:50′, 1:40′, 2:30′ and 3:20′ from the beginning of the experiment, with a rate of 0.5 L min^{-1}. Each water application lasted 20 min. The GPR surveys alternated with water applications, and occurred at 0:30′, 1:20′, 2:10′, 3:00′ and 3:50′ from the beginning of the experiment for SL1, and for SL2 at 0:40′, 1:30′, 2:20′, 3:10′ and 4:00′ from the beginning of the experiment.

During the second stage, five stemflow pulses, each of 10 L, were poured into the funnels connected to Trees 3, 4, and 5 at a rate of 0.5 L min^{-1}. Water additions were performed 4:20′, 5:00′, 5:40′, 6:20′ and 7:00′ from the beginning of the experiment. The other five GPR surveys again occurred after each water applications, at 4:40′, 5:20′, 6:00′, 6:40′ and 7:20′ from the beginning of the experiment for SL1, and for SL2 at 4:50′, 5:30′, 6:10′, 6:50′ and 7:30′ from the beginning of the experiment.

Overland flow was collected by small V-shaped aluminum channels placed into a groove previously scraped on the downhill side of the five trees (Fig. 2d). The water volumes were firstly collected in 25 L cans and then, after the experiment, measured by graduated beakers. Given that only the 0.3 % of the applied stemflow generated overland flow, while the majority infiltrated into the soil (99.7 %), these data are not presented in the result section.

2.3. Estimation of subsurface flow velocity

We also estimated approximate values of subsurface flow velocity (V_{SF} = velocity of first appearance of reflection changes at the GPR survey lines). The time was calculated between the time when stemflow artificial experiment started and the first reflection changes appearance (Weiler and McDonnell, 2007). The length of the preferential flow path was calculated as the linear distance along the slope direction between the GPR survey line and the nearest upslope tree. We considered the nearest upslope tree for the length calculation because it was not possible to determine the true source of the preferential flow paths among the trees involved during the stemflow simulation experiment. The experimental setup, on the other hand, was designed to differentiate between the preferential flow paths activated by the trees involved during the first stage (Trees 1, 2) and those involved during the second stage (3, 4, 5). In addition, because the true path is likely tortuous, the linear distance is a minimum distance generating maximum V_{SF} values.

2.4. Dye-staining experiment

Direct observation of the wetting patterns after the simulation was necessary to corroborate the role played by the course roots in promoting subsurface lateral flow. Therefore, we performed an additional artificial stemflow experiment using a dye tracer followed by destructive soil excavation to expose the dyed patterns. Since the Calderona site is a long-term monitoring experimental area (in which major soil disturbance is discouraged), for this test we selected an Aleppo pine tree located at around 0.7 m from a roadcutbank just outside of the experimental site. The roots observed on the roadcut were characterized by recording their diameter and depth. We applied on the tree trunk five stemflow pulses of brilliant blue dye (E133) solution (4 g L^{-1}), with each

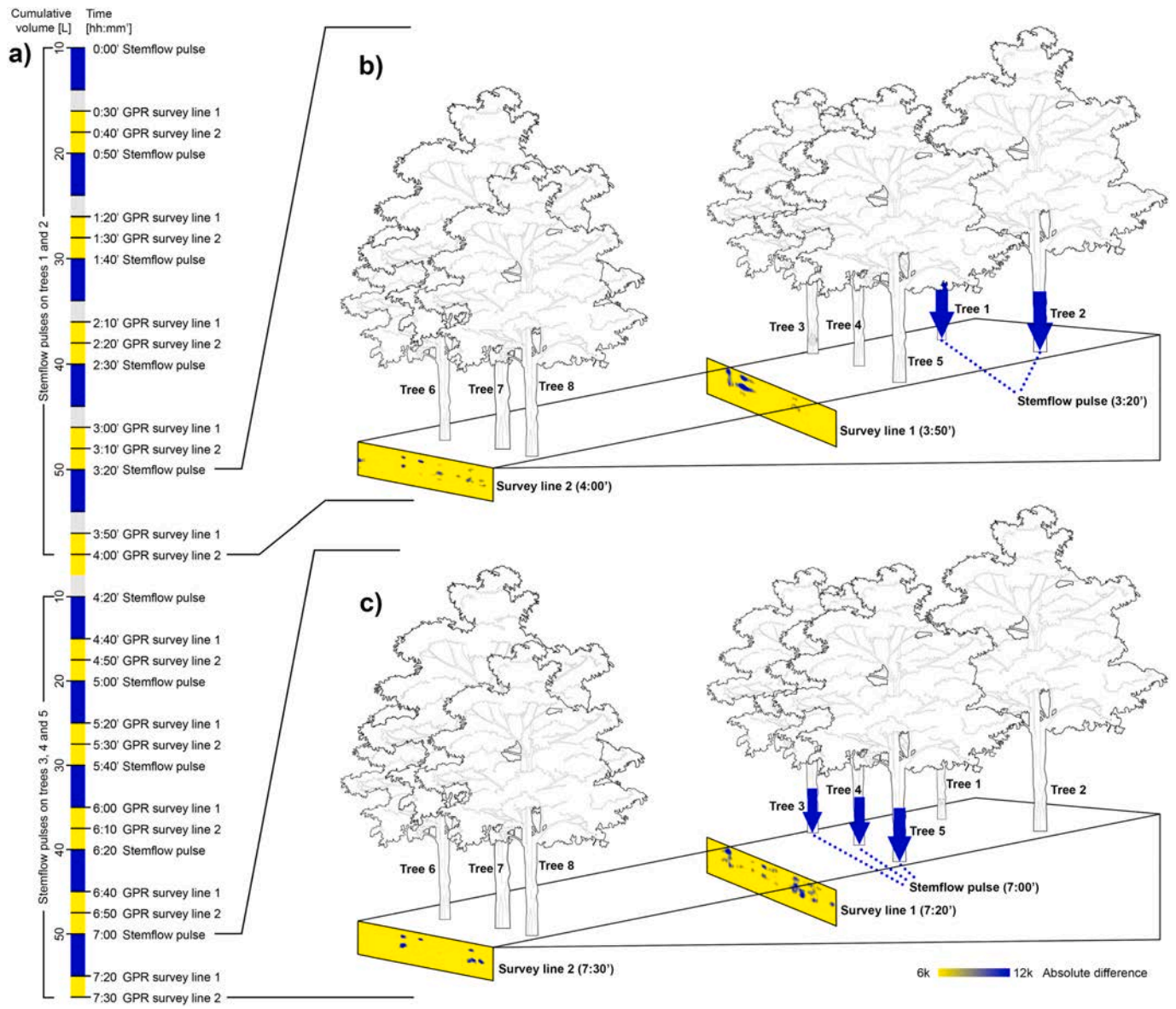

Fig. 3. (a): Timeline of the repeated GPR surveys and stemflow pulses. (b): Differenced radargrams obtained at the end of the first stage of the artificial stemflow experiment, when water was poured on Trees 1 and 2 (blue arrows) at time 3:50′ for Survey line 1 and 4:00′ for Survey line 2. (c): Differenced radargrams obtained at the end of the second stage of the artificail stemflow experiment, when water was poured on Trees 3, 4, and 5 (blue arrows) at time 7:20′ for Survey line 1 and 7:30′ for Survey line 2. (For interpretation of the references to colour in this figure legend, the reader is referred to the web version of this article.)

pulse consisting of 10 L. Two GPR surveys were carried out before and after the execution of the stemflow simulation on a 1.5 m-long survey line. At the end of the experiment, we photographed the dyed pattern and recorded its position and extension.

2.5. GPR data processing

We processed each collected radargram (i.e., a time-depth cross-section) using the Reflexw software version 9.5 (Sandmeier Scientific Software, Karlsruhe, Germany). The processing steps included: **i)** a reflection trace (A-scan) interpolation for obtaining an equal distance (e.g., equal number of traces) between the marks taken every 0.2 m, **ii)** a static time shift to align direct ground wave arrival to 0 ns, **iii)** an energy decay filter to compensate GPR energy attenuation with propagation depth, **iv)** a subtract-mean filter for eliminating low frequency parts (dewow), **v)** an average xy-filter for removing both distance- and time-dependent noise, and **vi)** a compression to reduce the sizes of the final matrixes.

To determine the appropriate velocity for converting two-way travel times into actual depths we performed a Common-Mid-Point (CMP) acquisition. Based on the determined velocity profile, we assumed in our analysis a uniform wave velocity of $V = 0.18$ m ns^{-1}. In addition, we confirmed the estimated velocity by measuring the real depth of the observed roots at the roadcut section which were also detected by the GPR. More specifically, we calculated the wave velocity as $V = 2 \times D/t$, where D (L) is the measured depth of observed roots and t (T) is the two-ways travel time in correspondence of the hyperbola vertex. Coarse roots are manifested as reflection hyperbolas because of the conical shape of the emitted radiowave signals. Indeed, previous work has demonstrated that when the antenna moves along a survey line approaching a root (target), the two-way travel time decreases towards its minimum value coinciding with the position of the antenna vertically above the target; then, as the antenna moves away from the target, the two-way travel time increases (Guo et al., 2013). Finally, we checked the estimated velocity through hyperbola adaptations.

Using this approach, we obtained one pre-wetting and ten post-

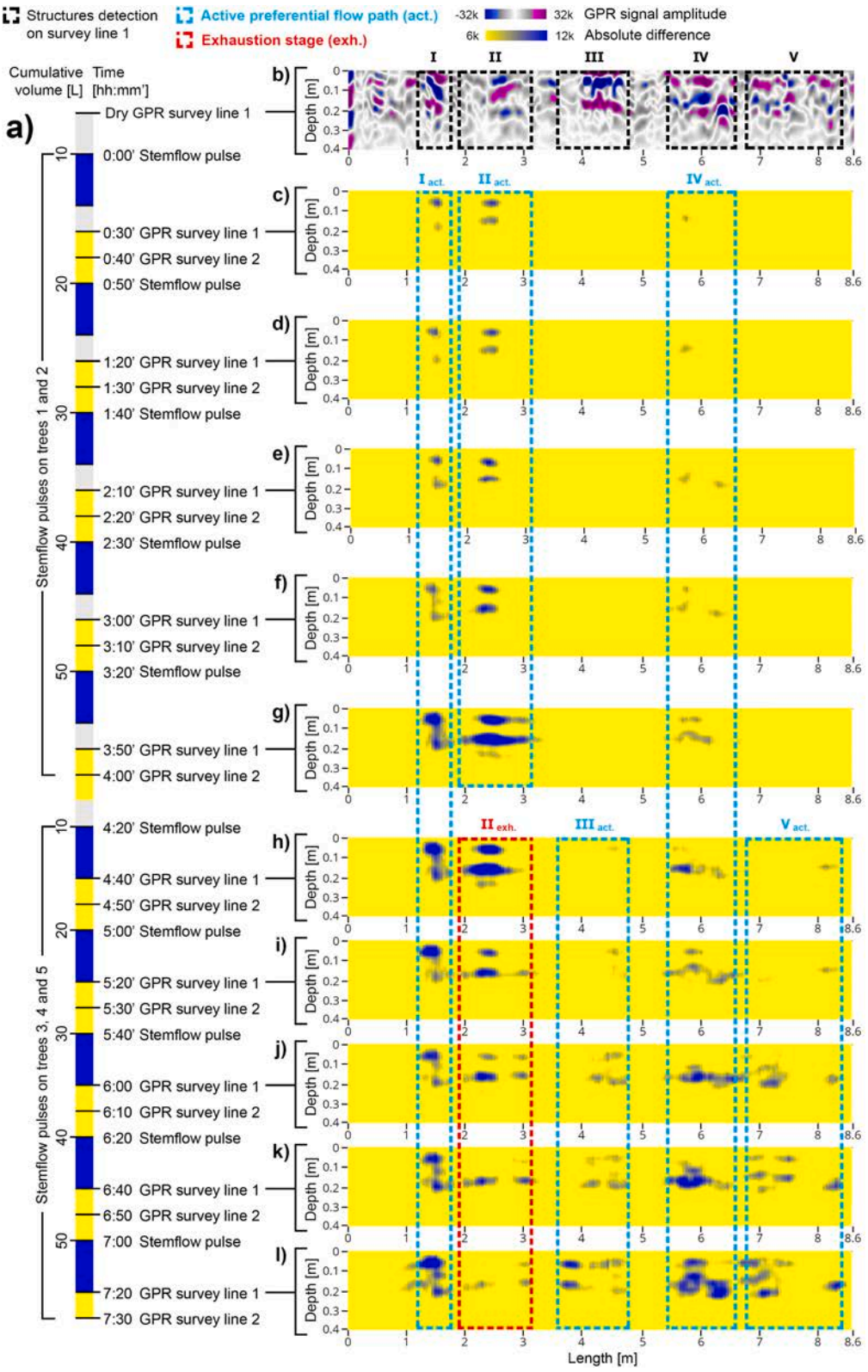

Fig. 4. (a): Timeline of the repeated GPR surveys and stemflow pulses for the GPR Survey line 1. (b): Radargram collected before the excution of the artificial steamflow experiment. (c-g): Differenced radargrams obtained during the first stage of the artificial stemflow experiment, when water was poured on Trees 1 and 2. (h-l): Differenced radargrams obtained during the second stage of the artificail stemflow experiment, when water was poured on Trees 3, 4 and 5. The positions of the coarse roots that triggered preferential flow paths are indicated with Roman numerals from I to V and black rectangles. The positions of the detected active preferential flow paths are indicated with Roman numerals followed by the subscrit act. (active) and blue rectangles. The exhaustion stages are indicated with Roman numerals followed by the subscrit exh. (exhaustion) and red rectangles. (For interpretation of the references to colour in this figure legend, the reader is referred to the web version of this article.)

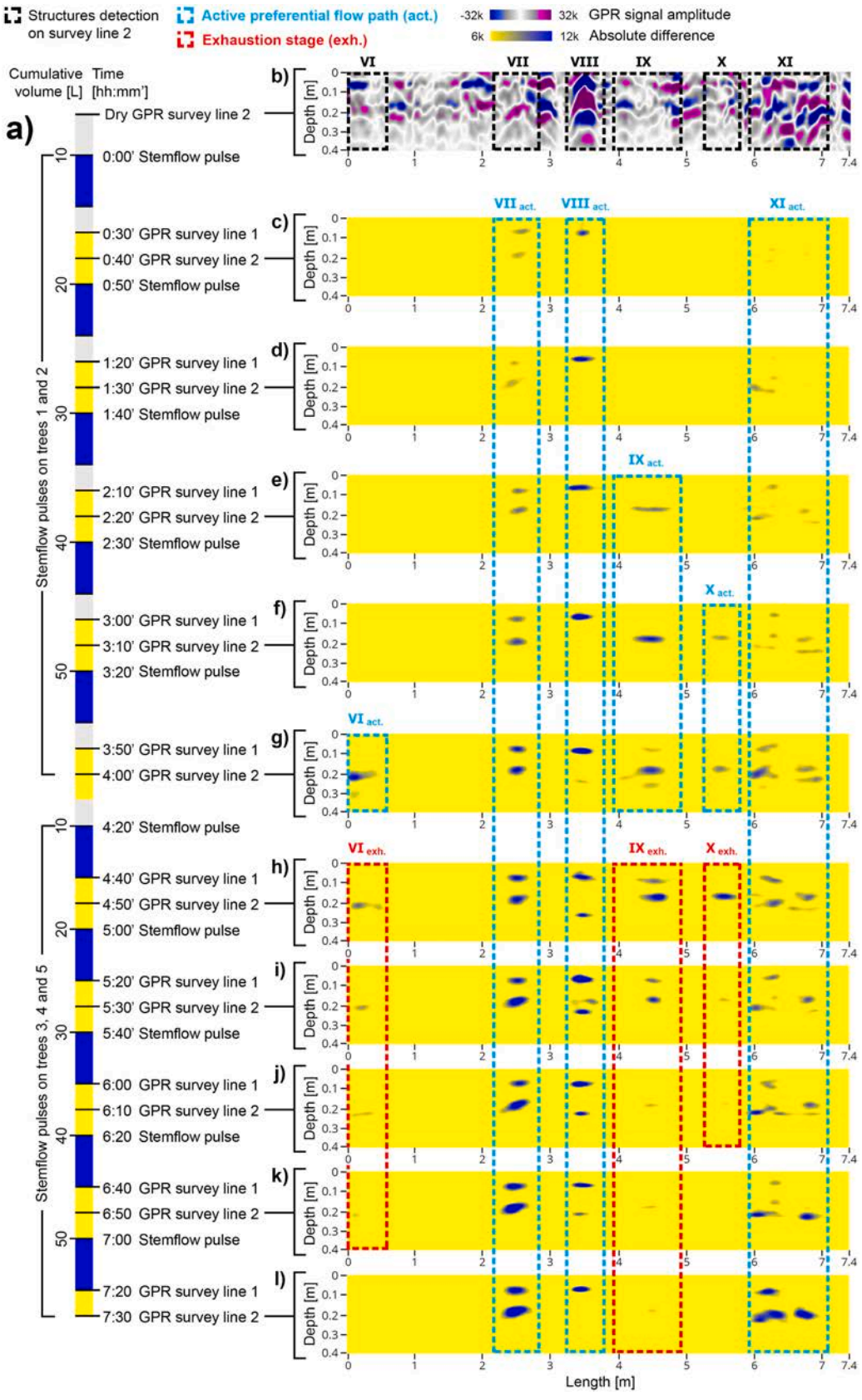

Fig. 5. (a): Timeline of the repeated GPR surveys and stemflow pulses for the GPR Survey line 2. (b): Radargram collected before the excution of the artificial steamflow experiment. (c-g): Differenced radargrams obtained during the first stage of the artificial stemflow experiment, when water was poured on Trees 1 and 2. (h-l): Differenced radargrams obtained during the second stage of the artificial stemflow experiment, when water was poured on Trees 3, 4 and 5. The positions of the coarse roots that triggered preferential flow paths are indicated with Roman numerals from VI to XI and black rectangles. The positions of the detected active preferential flow paths are indicated with Roman numerals followed by the subscrit act. (active) and blue rectangles. The exhaustion stages are indicated with Roman numerals followed by the subscrit exh. (exhaustion) and red rectangles. (For interpretation of the references to colour in this figure legend, the reader is referred to the web version of this article.)

wetting radargrams for each survey line. Next, we created other ten matrixes based on absolute differences between pre- and post-wetting amplitude values. Higher differenced values occurred as a consequence of amplitude changes and time shifts. Specifically, water imbibition by the soil caused a variation of the dielectric contrast between layers. This variation altered the reflection coefficient and caused the amplitude changes. Time shifts occurred because the water imbibition caused an increase in bulk dielectric constant, which reduced the velocity and increased the two-way travel time. As a consequence the reflectors appeared at later recording times as the soil became wet (Truss et al., 2007).

3. Results

3.1. Detection of preferential flow pathways

For each survey line, the first five differenced matrixes highlighted amplitude fluctuations during the first stage of the artificial stemflow experiment, when the stemflow pulses were poured on Trees 1 and 2 (Fig. 3b), whereas the last five differenced matrixes highlighted amplitude fluctuations during the second stage, when the stemflow pulses were poured on Trees 3, 4 and 5 (Fig. 3c).

Fig. 4c-l shows reflection changes that occurred during the whole infiltration experiment on SL 1. During the first stage of water application, when stemflow pulses were applied on Trees 1 and 2, we observed significant difference on three different zones (blue rectangles and Roman numerals **$I_{act.}$**, **$II_{act.}$** and **$IV_{act.}$** in Fig. 4c, where the subscript act. stands for active preferential flow path) with moderate increase in signal amplitude 30 min after infiltration started, i.e., after the first stemflow pulse. During the second stage of water application, when stemflow pulses were applied on Trees 3, 4, and 5, two other zones (blue rectangles and roman numerals **$III_{act.}$** and **$V_{act.}$** in Fig. 4h) showed reflection changes 20 min after the first stemflow pulse of the second series (280 min from the beginning of the experiment). On Survey line 2, all reflection changes started to appear during the first stage of water application, when stemflow pulses were applied on Trees 1 and 2 (Fig. 5c-g). More specifically, we measured reflection changes on three different zones (blue rectangles and numerals **$VII_{act.}$**, **$VIII_{act.}$** and **$XI_{act.}$** in Fig. 5c) with moderate increase in signal amplitude 40 min after infiltration started, i.e., after the first stemflow pulses. Three other zones showed reflection changes later during the experiment, occurring at 140 (blue rectangle and numeral **$IX_{act.}$** in Fig. 5e), 190 (blue rectangle and **$X_{act.}$** in Fig. 5f) and 240 min (blue rectangle and **$VI_{act.}$** in Fig. 5g) after infiltration started.

Using the data in Figs. 4 and 5, we also estimated approximate values of subsurface flow velocity (V_{SF}). The estimated V_{SF} values ranged from 1.9×10^3 to 1.2×10^4 mm h^{-1} (Table 1). These values do not reflect the velocity through the macropores, but integrate the mean velocity of the infiltrated stemflow along its flow path through the hillslope to the survey lines (Anderson et al., 2009).

Table 1
Values of subsurface flow velocity (V_{SF}).

Survey line	Tree	Preferential path	L [m]	Time [min]	V_{SF} [mm h^{-1}]
1	1–2	I $_{act.}$	2.77	30	5.5×10^3
		II $_{act.}$		30	5.5×10^3
		IV $_{act.}$		30	5.5×10^3
	3–4-5	III $_{act.}$	1.15	20	3.5×10^3
		V $_{act.}$		20	3.5×10^3
2	1–2	VI $_{act.}$	7.7	240	1.9×10^3
		VII $_{act.}$		40	1.2×10^4
		VIII $_{act.}$		40	1.2×10^4
		IX $_{act.}$		140	3.3×10^3
		X $_{act.}$		190	2.4×10^3
		XI $_{act.}$		40	1.2×10^4

3.2. Detection of coarse roots

Comparison between the differenced (Figs. 4c-l and 5c-l) and pre-wetting (Figs. 4b and 5b) radargrams collected on Survey lines 1 and 2 allowed us to identify the source of spatial heterogeneity that triggered preferential flow paths (black rectangles and Roman numerals **I**, **II**, **III**, **IV**, **V** in Fig. 4b and **VI**, **VII**, **VIII**, **IX**, **X**, **XI** in Fig. 5b). On the pre-wetting radargrams, hyperbolic reflections were associated to coarse roots growing perpendicular to the survey lines, which were oriented parallel to the slope direction (e.g., **IV** in Fig. 4b and **VIII** in Fig. 5b). These coarse roots triggered preferential flow paths that were manifested as strongest reflection differences on the differenced radargrams (e.g., blue rectangles **$IV_{act.}$** in Fig. 4c-l and **$VIII_{act.}$** in Fig. 5c-l). In some cases, reflection changes due to moisture variations were also detected in correspondence of reflectors that did not show a clear hyperbolic shape (e.g., blue rectangles and Roman numerals **$I_{act.}$**, **$II_{act.}$**, **$III_{act.}$**, **$V_{act.}$** in Fig. 4c-l and **$VI_{act.}$**, **$VII_{act.}$**, **$IX_{act.}$**, **$X_{act.}$**, **$XI_{act.}$** in Fig. 5c-l). More specifically, these isolated reflectors were associated with coarse roots that obliquely crossed the survey lines (e.g., numeral **I** in Fig. 4b and **VII** in Fig. 5b). Multiple reflectors, by contrast, were associated with the presence of many roots of different size and orientation (e.g., numeral **V** in Fig. 4b and **XI** Fig. 5b).

3.3. Dye-staining experiment

The dye-staining experiment was aimed at providing evidence of root-induced preferential flow. During the artificial stemflow experiment, the dye tracer was observed flowing along a 0.01-m-diameter root located at a depth of 0.31 m along the roadcut section (red rectangles in Fig. 6a-c). Thus, a certain volume of stemflow arriving from the tree trunk was funneled by this root as lateral subsurface flow. Reflection traces (A-scans) collected before and after the execution of the artificial stemflow experiment at 0.75 m of the survey line (X direction) also indicate this preferential water movement (Fig. 6e and g). Here, the reflection change measured at a depth of ~ 0.3 m coincides with the position of the root that funneled the dyed stemflow water (red rectangles in Fig. 6).

The radargrams (B-scans) collected before and after the execution of the artificial stemflow experiment also showed changes due to subsurface water movement (Fig. 6d and f). At 0.7 m of the survey line (x-direction), the prewetting radargram shows a main reflection hyperbola (yellow cross in Fig. 6d), corresponding to an observed coarse root with a diameter of 0.07 m (yellow cross in Fig. 6a). Within the same zone, we measured strong reflection changes at a depth of 0.05–0.2 m (Fig. 6h). Here, the infiltrated water extended within the downhill border of roadcut section without generating lateral flow but revealed a zone of imbibition surrounding the coarse root in the proximity of the trunk base. Consequently, no dye patches were observed at this 0.05–0.2 m depth interval.

4. Discussion

4.1. Evidence of flow connectivity

The analysis of the differenced radargrams allowed us to develop a conceptual model that explains the signals obtained for SL1 (Fig. 7). This model identifies three different cases that occurred during the activation of stemflow-induced preferential flow paths during the two stages of the infiltration experiments. Note that the delineated paths in Fig. 7 are hypothetical because, as discussed above (section 2.3), it was not possible to determine from which trees the preferential flow paths originated.

In the first case, we identified a preferential flow path crossing SL1 via detection of the wet patch indicated with the numeral **$II_{act.}$** in Fig. 7a. This flow path was activated during the first stage of the experiment by the stemflow infiltrated from Tree 1. During this stage, the signal

amplitude increased until achieving maximum differences between pre- and post-wetting conditions after the fifth stemflow pulse, i.e., 230 min after infiltration started (Fig. 4c-g, numeral $\mathbf{II_{act.}}$). This change in behavior signaled that the partially saturated (transmission) zone surrounding the fast-flow region had achieved its maximum extension. In this zone, the water pressure head decreased as the wetting front moved away due to soil capillarity and imbibition of water from preferential paths (Di Prima et al., 2022). Thus, although water mainly moved along preferential flow paths, infiltrated water also moved outward from stems due to water exchange between preferential flow pathways and matrix regions (Lassabatere et al., 2019, 2014). This process was influenced by the pressure gradient (Akay et al., 2008), thus, we can expect higher rates of water exchange between the two regions under drier conditions. On the contrary, lower rates are expected under initially wetter conditions and during natural storms, that is when water also infiltrates from the soil surface. More specifically, when it rains the advancement of the wetting front through the soil matrix changes the water content in the matrix pore system, and consequently, the water exchange rate between the two regions (Gerke and Genuchten, 1993).

During the second experimental stage, when water was poured on Trees 3–5, the signal amplitude decreased signaling the occurrence of an exhaustion stage (Fig. 4h-l, numeral $\mathbf{II_{exh.}}$, where the subscript exh. stands for exhaustion stage), with a general reduction of soil moisture within and around the feature (Fig. 7a, numeral $\mathbf{II_{exh.}}$ and red line). This observation implies that this preferential path was only activated when stemflow infiltrated from the upslope trees (e.g., Tree 1 in the hypothetical example in Fig. 7). This dynamic was also detected in correspondence to the wet patches $\mathbf{VI_{act.}}$– $\mathbf{VI_{exh.}}$, $\mathbf{IX_{act.}}$ –$\mathbf{IX_{exh.}}$ and $\mathbf{X_{act.}}$ –$\mathbf{X_{exh.}}$ of SL2 (Fig. 5).

In the second example, we consider the preferential flow path crossing SL1 that corresponds to the detected wet patch indicated with numeral $\mathbf{IV_{act.}}$ in Fig. 7b. This flow path was activated during the first stage of the experiment by the stemflow infiltrating from Tree 2. However, the signal amplitude also continued to increase during the second stage of the experiment (Fig. 4h-l, numeral $\mathbf{IV_{act.}}$), thereby providing evidence that infiltrating water from Trees 3–5 (e.g., Tree 5 in the hypothetical example in Fig. 7b) helped to keep this preferential flow path active. From this observation, we deduced that the two paths that are hydraulically connected with Trees 2 and 5 intersect each other at some point in the subsurface and form a network node (Fig. 7b). Thus, while we observed a constant increase of the signal amplitude at SL1 during the second stage (Fig. 7b, numeral $\mathbf{IV_{act.}}$), the branch of the network extending from the node to Tree 2 likely experienced an exhaustion stage (Fig. 7b, red line). We can hypothesize that this node is located somewhere downslope from Tree 5 or it may also coincide with Tree 5 location. In the latter case, during a natural storm, the stemflows infiltrated from Trees 2 and 5 converge directly below the Tree 5 location. This second dynamic was also detected as revealed by the wet patches $\mathbf{I_{act.}}$ of SL1 (Fig. 4), and $\mathbf{VII_{act.}}$, $\mathbf{VIII_{act.}}$ and $\mathbf{XI_{act.}}$ of SL2 (Fig. 5).

In the third case, we consider a preferential flow path crossing SL1 that was detected from the wet patch indicated with numeral $\mathbf{III_{act.}}$ in Figs. 7c and 4. This flow path was activated only during the second stage of the experiment by the stemflow infiltrated from Tree 3–5, thereby providing evidence that one or more of these trees acted as the source of this preferential flow path (e.g., Tree 4 in the hypothetical example in Fig. 7c). This second dynamic was also detected in correspondence of the wet patch $\mathbf{V_{act.}}$ of SL1 (Fig. 4h-l).

4.2. Comparison with previous measurements of lateral subsurface flow

Our findings allowed us to conceptualize the subsurface flow dynamics at the Calderona site and to support the hypothesis made by del Campo et al. (2019) about the presence of preferential flow networks affecting the hydrological response of the hillslope. The del Campo et al. (2019) study was focused on long-term monitoring activity at the experimental site that spanned the period from the 1st of October 2013

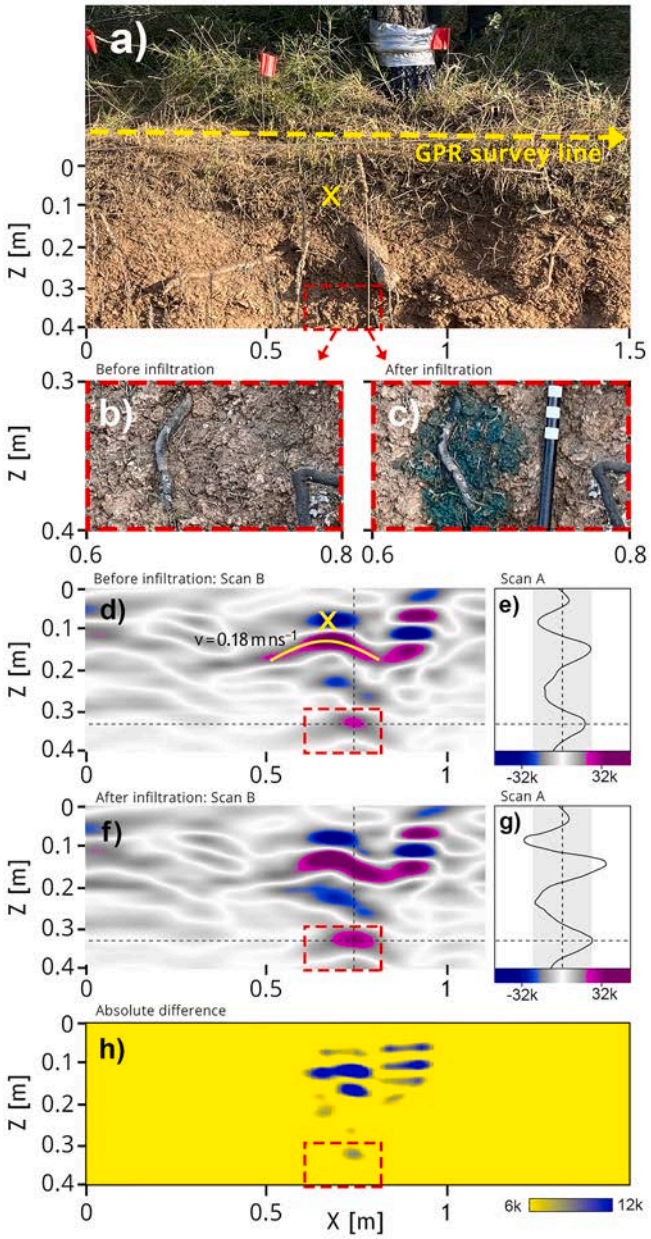

Fig. 6. Dye-staining experiment. (a): Roadcutbank with the selected Aleppo pine tree located at around 0.7 m from the border. The dashed yellow arrow demarcates the 1.5-m-long survey line positioned at a distance of 0.3 m from the roadcutbank. A root that funneled the stemflow were photographed (b) before and (c) after the appearance of the brilliant blue dye (E133) solution. Radargrams (B-scans) were collected on a 1.5-m-long survey line (d) before and (f) after the execution of the artificial stemflow experiment. Reflection traces (A-scans) were collected (e) before and (g) after the execution of the artificial stemflow experiment in correspondence of the root that funneled the dye tracer. (h): Differenced radargram. The red rectangles demarcate the position of the root that funneled the stemflow. The yellow cross demarcates the position of a coarse root and of the corresponding adapted hyperbola. (For interpretation of the references to colour in this figure legend, the reader is referred to the web version of this article.)

to the 30th of September 2016. As an example of the likely presence of stemflow-induced preferential flow, we selected two events from their work, one on the 9th of May 2016 and the other one on the 10th of August 2016, which produced 12 and 15 mm of subsurface lateral flow after 17 and 19 mm rainfalls. The maximum recorded rainfall intensities were 4.2 mm h^{-1} for the first event and 8.6 mm h^{-1} for the second ($\Delta t =$ 30 min). During these events subsurface lateral flow and increased water

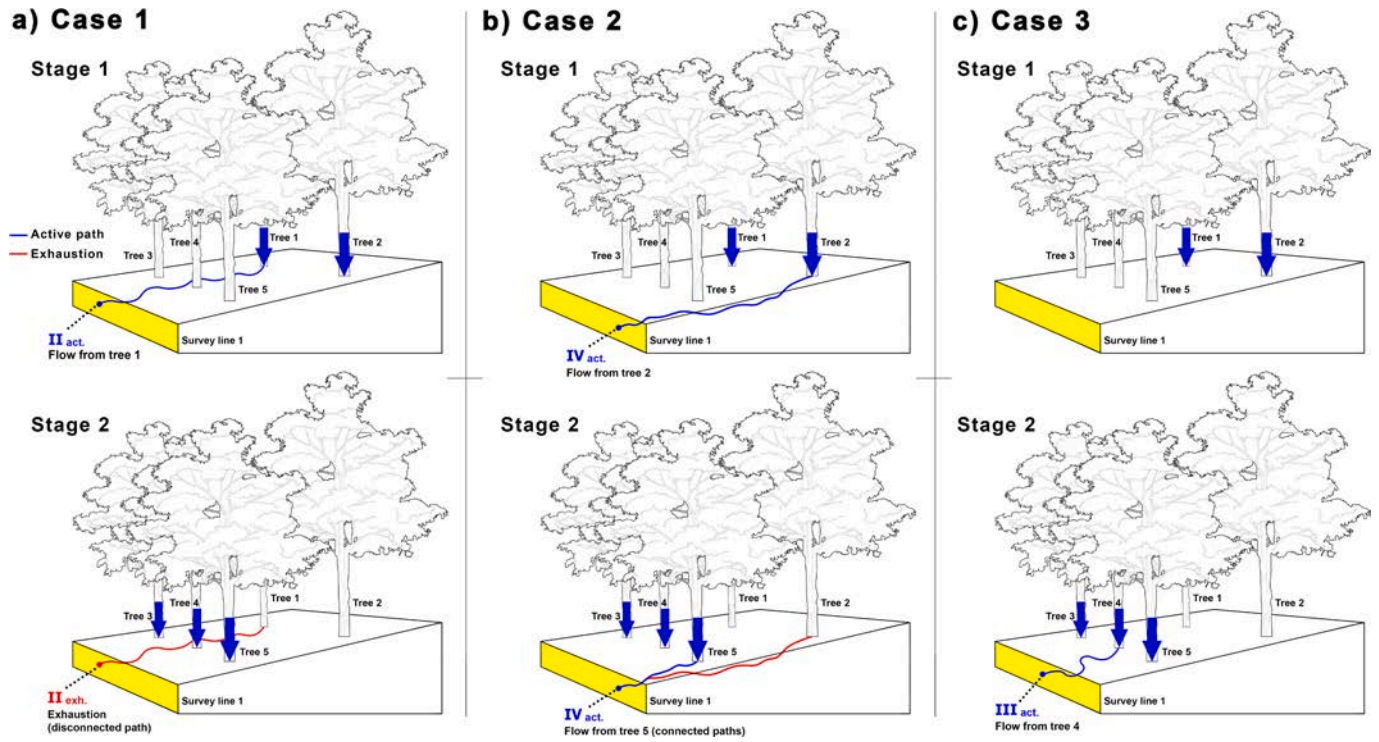

Fig. 7. Graphical example of three different cases of activation of stemflow-induced preferential flow paths (a, b and c). The example depicts preferential flow paths activated during the artificial stemflow experiment, when water was poured (blue arrows) on Trees 1 and 2 (Stage 1) and then on Trees 3, 4 and 5 (Stage 2). (For interpretation of the references to colour in this figure legend, the reader is referred to the web version of this article.)

levels in the piezometers were detected almost immediately after the onset of rainfall (Fig. 8), signaling the presence of preferential flow networks with a high capacity to drain the soil in both the lateral and vertical directions. The subsurface velocity values in Table 1 are in line with the rapid hydrological response evidenced during these storms. In addition, they were comparable to those measured by tracer experiments in many other investigations. For instance, Noguchi et al. (1999) measured values of preferential flow velocity ranging from 8.6×10^3 to 1.4×10^4 mm h^{-1} through dye experiments conducted in a forested hillslope. However, while previous studies allowed measuring subsurface flow velocity using methods that are labor-intensive (e.g., Pirastru et al., 2022) or invasive and non-repeatable (e.g., Noguchi et al., 1999), the present approach offered a non-invasive (or minimally invasive), repeatable, and accurate way to investigate subsurface flow in hillslopes, to detect preferential flow paths and to estimate flow velocities. Given these realistic velocities and the flashy response observed in Fig. 8, it is likely that stemflow infiltration is a main factor involved in lateral preferential flow initiation at the Calderona experimental site, in line with our main hypothesis. The rate at which stemflow accumulates depends on storm characteristics as well as tree size (crown and coarse roots) (Levia and Frost, 2003). The latter can be affected by forest management, which highlights the importance of water-oriented forest treatments (del Campo et al., 2014). The study site has been subjected to two forest management strategies. One plot was allowed to naturally regenerate following a wildfire in 1992, whereas another plot was controlled by strategically removing trees to limit tree density. Previous work in this site (del Campo et al., 2018, 2019) revealed that medium-large-sized trees in the thinned plot showed higher stemflow volume (2.3 and 1.7 L $tree^{-1}$ in thinning and control respectively), greater stemflow coefficients (0.44 and 0.30 L $tree^{-1}$ in thinning and control respectively), and more deep drainage than the un-thinned plot.

5. Summary and conclusions

In this study, the time-lapse GPR surveys carried out during the artificial stemflow experiment allowed us to detect stemflow-induced preferential flow paths activated by different trees and the related hydrological connectivity at the hillslope spatial scale. To our knowledge, this is the first study that gets insight on this process at the hillslope scale, involving five trees in the stemflow artificial experiment. The analysis of the differenced radargrams helped us to identify different dynamics in the initiation of lateral preferential flow, including the activation of connected preferential flow paths that received stemflow water from different trees during the simulation. These observations provided empirical evidence of preferential flow networks induced by root systems, and also their interconnection and contributions to flashy responses of the hillslope. These findings also imply that considering stemflow infiltration in hillslope hydrological models would improve our capacity to simulate and predict subsurface flow processes. The results can also help to guide specific forest treatments in these semiarid forests than enhance water retention and provisioning. The applied protocol can be used to gain more comprehensive understanding of the ecohydrological role played by stemflow infiltration.

CRediT authorship contribution statement

Simone Di Prima: Conceptualization, Methodology, Investigation, Data curation, Formal analysis, Validation, Visualization, Writing – original draft, Writing – review & editing, Funding acquisition. **Gersende Fernandes:** Investigation, Writing – review & editing. **Elisa Marras:** Investigation, Writing – review & editing. **Filippo Giadrossich:** Investigation, Writing – review & editing. **Ryan D. Stewart:** Investigation, Writing – review & editing. **Majdi R. Abou Najm:** Investigation, Writing – review & editing. **Thierry Winiarski:** Investigation, Writing – review & editing. **Brice Mourier:** Investigation, Writing – review & editing. **Rafael Angulo-Jaramillo:** Investigation, Writing – review & editing. **Alessandro Comegna:** Writing – review & editing. **Antonio del Campo:** Writing – review & editing, Funding acquisition. **Laurent Lassabatere:** Investigation, Writing – review & editing, Funding acquisition.

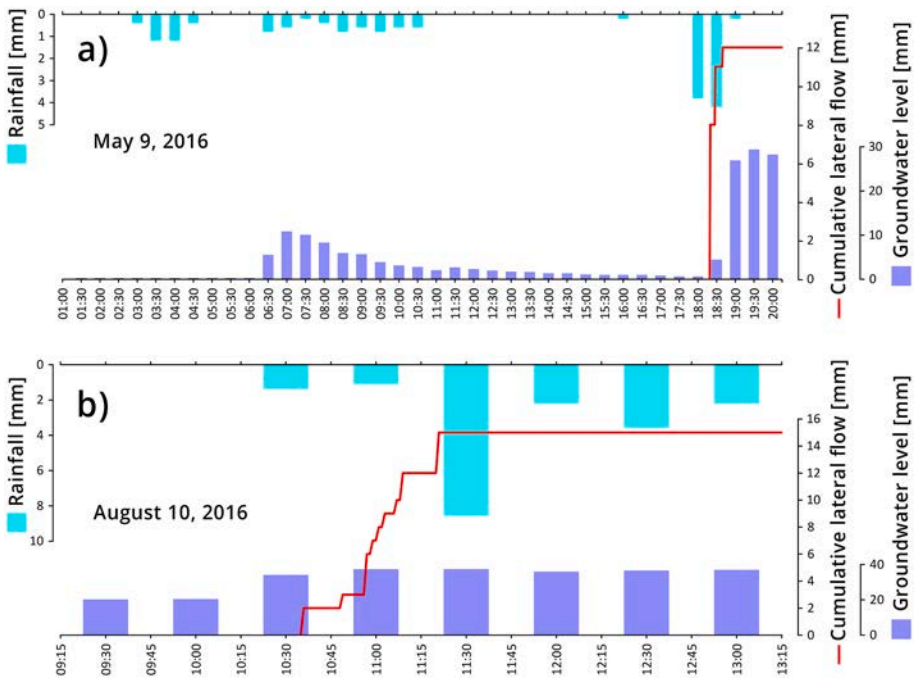

Fig. 8. Data from del Campo et al. (2019) showing cumulative lateral subsurface flow collected by a trench excavated downslope from the plot to a depth of 0.4 m (the same depth was considered in this study for geophysical inspections), and groundwater levels measured on four piezometers excavated at the downslope side of the trench. These wells were aimed at checking the groundwater level and the interaction between vertical (deep drainage) and lateral flow.

Declaration of Competing Interest

The authors declare that they have no known competing financial interests or personal relationships that could have appeared to influence the work reported in this paper.

Data availability

Data will be made available on request.

Acknowledgements

The authors thank Maria Burguet Marimon, Daniel Donze, Rim Maamouri and Imen Mhimdi for their contribution during the field activity. S.D.P. also thanks the H.F.C. and S.O.W. for their contribution to keeping everyone's spirits up and Toni for helping in a moment of need.

Funding

This work was supported through: i) the MIUR Project (PRIN 2020) "Unravelling interactions between WATER and carbon cycles during drought and their impact on water resources and forest and grassland ecosySTEMs in the Mediterranean climate" (WATERSTEM, protocol code: 20202WF53Z), ii) the European Regional Development Fund (ERDF) and the Italian Ministry of Education, University and Research (MIUR) through the "Programma Operativo Nazionale (PON) Ricerca e Innovazione 2014–2020" (Linea 1 - Mobilità dei ricercatori, AIM1853149, CUP: J54I18000120001), iii) the INFILTRON Project (ANR-17-CE04-0010, Package for assessing infiltration & filtration functions of urban soils in stormwater management), and iv) CEHYRFO-MED (CGL2017-86839-C3-2-R funded by MCIN/AEI /https://doi.org/10.13039/501100011033/ and FEDER).

References

Akay, O., Fox, G.A., Šimůnek, J., 2008. Numerical Simulation of Flow Dynamics during Macropore-Subsurface Drain Interactions Using HYDRUS. Vadose Zone Journal 7 (3), 909–918.

Anderson, A.E., Weiler, M., Alila, Y., Hudson, R.O., 2009. Subsurface flow velocities in a hillslope with lateral preferential flow. Water Resources Research 45. https://doi.org/10.1029/2008WR007121.

Bachmair, S., Weiler, M., 2011. New Dimensions of Hillslope Hydrology. In: Levia, D.F., Carlyle-Moses, D., Tanaka, T. (Eds.), Forest Hydrology and Biogeochemistry, Ecological Studies. Springer, Netherlands, Dordrecht, pp. 455–481. https://doi.org/10.1007/978-94-007-1363-5_23.

Calheiros, T., Pereira, M.G., Nunes, J.P., 2021. Assessing impacts of future climate change on extreme fire weather and pyro-regions in Iberian Peninsula. Science of The Total Environment 754, 142233. https://doi.org/10.1016/j.scitotenv.2020.142233.

Camarasa-Belmonte, A.M., Soriano, J., 2014. Empirical study of extreme rainfall intensity in a semi-arid environment at different time scales. Journal of Arid Environments 100–101, 63–71. https://doi.org/10.1016/j.jaridenv.2013.10.008.

del Campo, A.D., Fernandes, T.J.G., Molina, A.J., 2014. Hydrology-oriented (adaptive) silviculture in a semiarid pine plantation: How much can be modified the water cycle through forest management? European Journal of Forest Research 133, 879–894. https://doi.org/10.1007/s10342-014-0805-7.

del Campo, A.D., González-Sanchis, M., Lidón, A., Ceacero, C.J., García-Prats, A., 2018. Rainfall partitioning after thinning in two low-biomass semiarid forests: Impact of meteorological variables and forest structure on the effectiveness of water-oriented treatments. Journal of Hydrology 565, 74–86. https://doi.org/10.1016/j.jhydrol.2018.08.013.

del Campo, A.D., González-Sanchis, M., Molina, A.J., García-Prats, A., Ceacero, C.J., Bautista, I., 2019. Effectiveness of water-oriented thinning in two semiarid forests: The redistribution of increased net rainfall into soil water, drainage and runoff. Forest Ecology and Management 438, 163–175. https://doi.org/10.1016/j.foreco.2019.02.020.

Di Prima, S., Giannini, V., Ribeiro Roder, L., Giadrossich, F., Lassabatere, L., Stewart, R. D., Abou Najm, M.R., Longo, V., Campus, S., Winiarski, T., Angulo-Jaramillo, R., del Campo, A., Capello, G., Biddoccu, M., Roggero, P.P., Pirastru, M., 2022. Coupling time-lapse ground penetrating radar surveys and infiltration experiments to characterize two types of non-uniform flow. Science of The Total Environment 806, 150410. https://doi.org/10.1016/j.scitotenv.2021.150410.

Gerke, H.H., van Genuchten, M.T., 1993. A dual-porosity model for simulating the preferential movement of water and solutes in structured porous media. Water Resources Research 29, 305–319. https://doi.org/10.1029/92WR02339.

Guo, L., Chen, J., Cui, X., Fan, B., Lin, H., 2013. Application of ground penetrating radar for coarse root detection and quantification: a review. Plant Soil 362, 1–23. https://doi.org/10.1007/s11104-012-1455-5.

Guo, L., Mount, G.J., Hudson, S., Lin, H., Levia, D., 2020. Pairing geophysical techniques improves understanding of the near-surface Critical Zone: Visualization of

preferential routing of stemflow along coarse roots. Geoderma 357, 113953. https://doi.org/10.1016/j.geoderma.2019.113953.

Johnson, M.S., Lehmann, J., 2006. Double-funneling of trees: Stemflow and root-induced preferential flow. Écoscience 13, 324–333. https://doi.org/10.2980/i1195-6860-13-3-324.1.

Lassabatere, L., Di Prima, S., Bouarafa, S., Iovino, M., Bagarello, V., Angulo-Jaramillo, R., 2019. BEST-2K Method for Characterizing Dual-Permeability Unsaturated Soils with Ponded and Tension Infiltrometers. Vadose Zone Journal 18 (1), 1–20. https://doi.org/10.2136/vzj2018.06.0124.

Lassabatere, L., Yilmaz, D., Peyrard, X., Peyneau, P.E., Lenoir, T., Šimůnek, J., Angulo-Jaramillo, R., 2014. New Analytical Model for Cumulative Infiltration into Dual-Permeability Soils. Vadose Zone Journal 13 (12), 1–15. https://doi.org/10.2136/vzj2013.10.0181.

Lehmann, P., Hinz, C., McGrath, G., Tromp-van Meerveld, H.J., McDonnell, J.J., 2007. Rainfall threshold for hillslope outflow: an emergent property of flow pathway connectivity. Hydrology and Earth System Sciences 11, 1047–1063. https://doi.org/10.5194/hess-11-1047-2007.

Levia, D.F., Frost, E.E., 2003. A review and evaluation of stemflow literature in the hydrologic and biogeochemical cycles of forested and agricultural ecosystems. Journal of Hydrology 274 (1-4), 1–29.

Llorens, P., Domingo, F., 2007. Rainfall partitioning by vegetation under Mediterranean conditions. A review of studies in Europe. Journal of Hydrology 335, 37–54. https://doi.org/10.1016/j.jhydrol.2006.10.032.

Noguchi, S., Tsuboyama, Y., Sidle, R.C., Hosoda, I., 1999. Morphological Characteristics of Macropores and the Distribution of Preferential Flow Pathways in a Forested Slope Segment. Soil Sci. Soc. Am. J. 63, 1413–1423. https://doi.org/10.2136/sssaj1999.6351413x.

Pirastru, M., Iovino, M., Marrosu, R., Di Prima, S., Giadrossich, F., Awada, H., 2022. Large-scale lateral saturated soil hydraulic conductivity as a metric for the connectivity of subsurface flow paths at hillslope scale. Hydrological Processes 36, e14649.

Schwärzel, K., Ebermann, S., Schalling, N., 2012. Evidence of double-funneling effect of beech trees by visualization of flow pathways using dye tracer. Journal of Hydrology 470–471, 184–192. https://doi.org/10.1016/j.jhydrol.2012.08.048.

Truss, S., Grasmueck, M., Vega, S., Viggiano, D.A., 2007. Imaging rainfall drainage within the Miami oolitic limestone using high-resolution time-lapse ground-penetrating radar. Water Resour. Res. 43 https://doi.org/10.1029/2005WR004395.

Uchida, T., Kosugi, K., Mizuyama, T., 2001. Effects of pipeflow on hydrological process and its relation to landslide: a review of pipeflow studies in forested headwater catchments. Hydrol. Process. 15, 2151–2174. https://doi.org/10.1002/hyp.281.

Weiler, M., McDonnell, J.J., 2007. Conceptualizing lateral preferential flow and flow networks and simulating the effects on gauged and ungauged hillslopes. Water Resources Research 43. https://doi.org/10.1029/2006WR004867.